

**High-energy product  $\text{SmCo}_5@Fe$  core-shell nanoparticles**

L. L. Oliveira and Ana L. Dantas

*Department of Science and Technology, UERN, Natal, RN, Brazil*

S. S. Pedrosa and G. O. G. Rebouças

*Department of Physics, UFERSA, Angicos, RN, Brazil*

R. B. da Silva

*Department of Physics, UERN, Mossoró, RN, Brazil*

J. M. de Araújo and A. S. Carriço

*Department of Physics, UFRN, Natal, RN, Brazil*

(Received 22 January 2018; revised manuscript received 25 March 2018; published 16 April 2018)

We report a theoretical study of core-shell dipolar interaction effects on the energy product of hard/soft  $\text{SmCo}_5@Fe$  core-shell spherical nanoparticles. We show that the impact of the core-shell dipolar interaction on the shell reversal process is tunable by the values of the core diameter and shell thickness. Maximum energy product optimization requires small core diameters, and the energy product enhancement may reach more than 370% for small core diameters  $\text{SmCo}_5@Fe$  core-shell nanoparticles.

DOI: [10.1103/PhysRevB.97.134413](https://doi.org/10.1103/PhysRevB.97.134413)**I. INTRODUCTION**

Bimagnetic ferromagnetic systems made of exchange-coupled hard/soft core-shell (HSCS) nanoparticles and nanocomposites have been investigated as possible routes to producing new materials for high-energy product (HEP) magnets [1–9]. The motivation is the chance of tailoring the composition while granting an efficient exchange coupling of the hard and soft phases, combining the large anisotropy of the hard material, and the large magnetization of the soft material, to optimize the energy product  $(BH)_{\text{max}}$  [10].

Nanostructuring exchange-coupled ferromagnetic materials in small volumes holds good chances of tailoring the magnetic properties of nanosized systems. Confinement in small volumes affects the interplay of exchange and dipolar interactions, the magnetic phases, and the reversal mechanisms. The interest stems from both the chances of designing new systems for fundamental studies of magnetism in confined geometries and from the promising perspectives of new systems for a variety of emerging applications [1,11–13]. Efforts towards a more efficient control of exchange coupling as a function of the hard/soft materials phases content lead to nanocomposite systems for HEP permanent magnets applications composed of exchange coupled hard-soft nanoparticles [1,2].

The magnetic phases in the demagnetization quadrant and the reversal mechanism of the core-shell nanoparticles are key issues for optimizing the core-shell composition for high energy product materials applications. As we discuss presently, the core-shell dipolar interaction plays a key role in the structure of the magnetic phases and in the reversal mechanisms. Furthermore, the dipolar interaction is tunable by the values of the core diameter and the shell thickness.

The core dipolar field of spherical hard-soft core-shell nanoparticles is easily predictable. The large core anisotropy

favors a core uniform magnetization state in the demagnetization quadrant and qualifies the core as a stable dipolar field source at the shell [14]. Furthermore, materials with very high magnetocrystalline anisotropy, such as FePt,  $\text{SmCo}_5$ , and  $\text{Nd}_2\text{Fe}_{14}\text{B}$ , allow producing hard-soft core-shell nanoparticles with a wide range of core diameter values, starting with a few nanometers diameter core hard material nanoparticles [2]. As a result, spherical HSCS nanoparticles provide a rather special scenario for designing HEP materials, by proper choice of the core-shell composition.

For high-temperature applications,  $\text{SmCo}_5@Fe$  exchange coupled nanocomposites and  $\text{SmCo}_5@Fe$  core-shell nanoparticles are amongst the mostly investigated compositions.  $\text{SmCo}_5$  has a large anisotropy energy density of the order of  $10^8$  erg/cm<sup>3</sup> and a magnetization around 851.91 emu/cm<sup>3</sup>, while Fe has a magnetization twice as large (1711.78 emu/cm<sup>3</sup>), and much smaller anisotropy energy density of the order of  $10^5$  erg/cm<sup>3</sup> [15].

In this paper, we report a theoretical discussion of the impact of the core-shell dipolar interaction on the magnetic phases, the reversal mechanisms, and on the energy product of spherical  $\text{SmCo}_5@Fe$  core-shell nanoparticles. We consider  $\text{SmCo}_5(D)@Fe(\delta)$  core-shell nanoparticles with  $\text{SmCo}_5$  core diameter ( $D$ ) ranging from 3.5 nm to 21 nm and Fe shell thicknesses ( $\delta$ ) up to 8 nm. The key point is finding values of the  $\text{SmCo}_5$  core diameter and Fe shell thickness which leads to an optimum core-shell composition for HEP nanocomposite materials.

Using a simple average nanoparticle model, and focusing solely on the volume fractions of the core and shell materials, the optimization of the  $\text{SmCo}_5(D)@Fe(\delta)$  core-shell nanoparticle composition for HEP magnets would just require taking advantage of increasing the average magnetization by the addition of the Fe shell, while, at the same time,

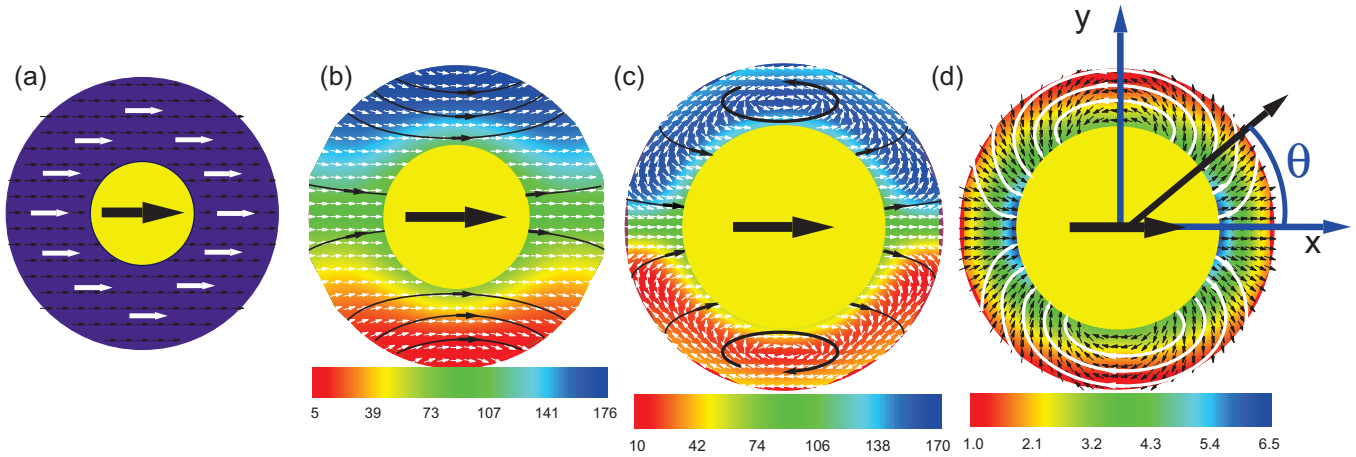


FIG. 1. (a) The magnetization pattern of  $\text{SmCo}_5(3.5 \text{ nm})@Fe(2.5 \text{ nm})$  core-shell nanoparticles for  $H = -10.31 \text{ kOe}$ . (b) and (c) shows the shell vortex phase magnetization pattern of the  $\text{SmCo}_5(11 \text{ nm})@Fe(6.0 \text{ nm})$  and  $\text{SmCo}_5(21 \text{ nm})@Fe(6.0 \text{ nm})$  core-shell nanoparticles for  $H = -5.35 \text{ kOe}$  and  $H = -12.5 \text{ kOe}$ . (d) The panel shows the  $\text{SmCo}_5(21 \text{ nm})@Fe(6.0 \text{ nm})$  core dipolar field pattern within the shell. The color barcode in (b) and (c) corresponds to the out-of-plane angle and in (d) corresponds to the strength of dipolar field in kOe.

minimizing the drop in the average anisotropy energy. However, the average HSCS nanoparticle model does not account for the shell relaxation, due to the core-shell dipolar interaction, and, as we shall discuss below, applies only for small values of the core diameter and shell thickness.

Theoretical [16] studies of small core diameter hard-soft core-shell nanoparticles, with modest values of the shell material saturation magnetization (from 100 to 500  $\text{emu}/\text{cm}^3$ ), revealed hysteresis loops displaying a nearly coherent magnetization reversal, and large reductions of the coercive field. In these cases, due to the small value of the shell magnetization, core-shell dipolar effects are weak, and the angular dependence of the switching field follows the Stoner-Wohlfarth reversal mode [16].

Interestingly, experimental reports on the maximum energy product of nanocomposites made of small diameter  $\text{FePt}@Fe_3O_4$  core-shell nanoparticles [8,17], using 4 nm to 8 nm diameters FePt core nanoparticles, revealed large size effects, with considerable reductions in the coercive field, and an energy product enhancement of around 38%, for shell thicknesses in the 1–3 nm range.

The reported large size effects and enhancement of the energy product, using a few nanometers thick small magnetization magnetite shells, with  $M_S \approx 480 \text{ emu}/\text{cm}^3$  [15], is indicative of a key feature. For small core diameter, large values of the percentage shell volume fraction may be reached with rather thin shells. As we shall discuss presently, this may be explored for the optimization of core-shell nanoparticles, with large magnetization shell materials, for high energy product applications. A strong ferromagnetic core-shell interface exchange energy is a key element for keeping core and shell magnetizations parallel, favoring coherent reversal with smooth hysteresis loops [8,17,18].

On the other hand, the core-shell dipolar interaction may compete with the interface exchange energy [14]. The long-ranged dipolar field produced by the core in the shell is opposite to the core magnetization, except for the shell region near the

poles of the core, and may produce nonuniform phases, as shown in Fig. 1.

The optimum design of exchange coupled HSCS nanoparticles for HEP applications is largely based on the assumption that the large core anisotropy material switches coherently, at large values of the external field strength, and holds the soft material shell via a strong ferromagnetic interface exchange energy. The anisotropic nature of the core dipolar field is a major issue for choosing the optimum value of the shell thickness  $\delta^*$  for a given value of the core diameter. HSCS nanoparticles may exhibit large variations in the magnetization of thin shells, due to the core dipolar field gradient within the shell [14].

As shown in Fig. 1 the core dipolar field in the shell is parallel to the core magnetization near the polar regions ( $|\delta\theta| \approx \pi/4$ , around the  $\theta = 0$  and  $\theta = \pi$  poles) and opposite to the core magnetization at the  $\theta \approx \pi/2$  belt. This built in dipolar field gradient favors a nonuniform magnetization profile at the shell. In the shell regions near the  $\theta \approx 0$  and  $\theta \approx \pi$  poles, the interface exchange coupling is reinforced by the core-shell dipolar interaction, while at the  $\theta \approx \pi/2$  belt, the exchange and dipolar energies favor opposite trends. This is a key issue, because it may trigger the nucleation of reversal for large values of the core diameter and the shell thickness.

We have found that for small core diameter nanoparticles with thin shells, the ferromagnetic core-shell exchange interaction prevails. However, as the core diameter and shell thickness increase, the long-ranged core-shell dipolar energy may overcome the short-ranged ferromagnetic exchange interaction. This may lead to noncoherent reversal for large values of the percentage shell volume fraction, imposing limits on the maximum energy product.

As we shall discuss below, for the  $\text{SmCo}_5(11 \text{ nm})@Fe(\delta)$  and  $\text{SmCo}_5(21 \text{ nm})@Fe(\delta)$  nanoparticles, the competition between the interface exchange and the dipolar energies, for large core diameter values, may lead to the formation of a new

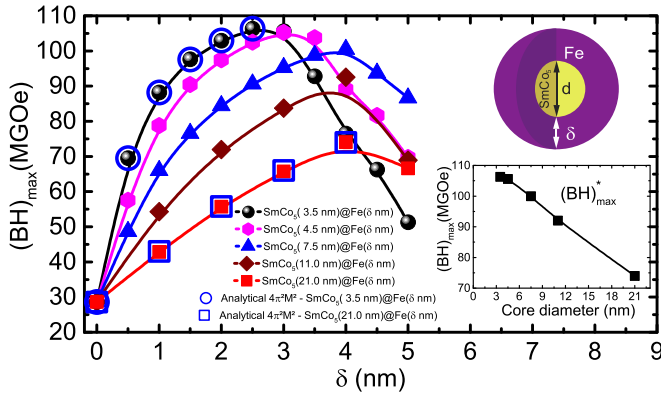


FIG. 2.  $(BH)_{\max}$  of  $\text{SmCo}_5(D)@Fe(\delta)$  core-shell nanoparticles, with core diameters  $D$  of 3.5, 4.5, 7.5, 11, and 21 nm, and Fe shells thicknesses  $\delta$  ranging from 0 to 5 nm. The full and open symbol curves show the values of  $(BH)_{\max}$  predicted by the current theoretical model, and the theoretical maximum value of the energy product,  $4\pi^2 M^2$ , for the  $\text{SmCo}_5(3.5 \text{ nm})@Fe(\delta)$  and  $\text{SmCo}_5(21 \text{ nm})@Fe(\delta)$  nanoparticles. In the inset we show the maximum value of the energy product for each one of the chosen  $\text{SmCo}_5$  cores.

magnetic phase, the shell vortex phase, in the demagnetization quadrant. In the shell vortex phase the core is uniformly magnetized and the shell displays a curling magnetization pattern that resembles to some extent the vortex phase of soft ferromagnetic materials.

3.5 nm core diameter  $\text{SmCo}_5(3.5 \text{ nm})@Fe(\delta)$  nanoparticles, with Fe shell thicknesses ( $\delta$ ) up to 8 nm, exhibit coherent reversal hysteresis curves, with the core and shell magnetizations exchange coupled. 21 nm core diameter  $\text{SmCo}_5(21 \text{ nm})@Fe(\delta)$  nanoparticles, with Fe shell thickness  $\delta$  ranging from 1 nm up to 8 nm, exhibit noncoherent reversal. As shown in Fig. 2, the maximum energy product  $(BH)_{\max}$  is a decreasing function of the core diameter value, dropping from 106.3 MGOe for the 3.5 nm core diameter  $\text{SmCo}_5(3.5 \text{ nm})@Fe(\delta)$  nanoparticles to 74.1 MGOe for the 21 nm core diameter  $\text{SmCo}_5(21 \text{ nm})@Fe(\delta)$  nanoparticles.

The  $\text{SmCo}_5(3.5 \text{ nm})@Fe(\delta)$  nanoparticle has an optimum shell thickness of  $\delta^* = 2.5$  nm, corresponding to a shell volume fraction of 93% and an energy product of 106.3 MGOe. This is 3.7 larger than the theoretical maximum value of the energy product ( $4\pi^2 M^2$ ) of  $\text{SmCo}_5$  (28.6 MGOe).

$\text{SmCo}_5(21 \text{ nm})@Fe(\delta)$  nanoparticles require a much thicker Fe shell in order to reach a percentage shell volume fraction comparable to the optimum composition of  $\text{SmCo}_5(3.5 \text{ nm})@Fe(\delta)$  nanoparticles. However, the 21 nm core diameter  $\text{SmCo}_5(21 \text{ nm})@Fe(\delta)$  nanoparticle has an optimum shell thickness of  $\delta^* = 4.0$  nm, corresponding to a modest 62% shell volume fraction and an energy product of 74.1 MGOe.

## II. THEORETICAL MODEL

We consider a single core-shell nanoparticle and assume that the  $\text{SmCo}_5$  core and the Fe shell have the uniaxial anisotropy along the  $x$  axis. The magnetic structure is described using small cubic cells with edge  $d$ , smaller than the domain wall width and exchange lengths of the core and shell materials.

The energy density is given by:

$$E = -H\hat{x} \cdot \sum_j M_S^j \hat{m}_j - \sum_j K^j (m_j^x)^2 + \frac{1}{2} \sum_j \sum_k M_S^j M_S^k \left( \frac{\hat{m}_j \cdot \hat{m}_k}{n_{jk}^3} - \frac{3(\hat{m}_j \cdot \hat{n}_{jk})(\hat{m}_k \cdot \hat{n}_{jk})}{n_{jk}^5} \right) + \frac{1}{d^2} \sum_j \sum_k A_{jk} (1 - \hat{m}_j \cdot \hat{m}_k). \quad (1)$$

The first two terms are the Zeeman and anisotropy energies,  $M_S^j$  is the  $j$ -cell saturation magnetization, and  $\hat{m}_j$  is the magnetization direction. In the dipolar energy,  $n_{jk}$  is the distance between the cells  $j$  and  $k$  in units of cell edge. The exchange energy couples nearest neighbor cells.  $A_{jk}$  is either the core or the shell exchange stiffness, for cells  $j$  and  $k$  within the same material, otherwise, it represents the effective interface exchange energy.

For each value of the external field  $H$ , the core-shell magnetization pattern is found using a self-consistent algorithm [11–14]. The magnetization  $\hat{m}_j$  is adjusted to be parallel to the effective magnetic field ( $H_{\text{eff}}^j = -(1/M_S)(\partial E/\partial \hat{m}_j)$ ), so that for each one of the cells the torque is smaller than  $10^{-17}$  erg.

For  $\text{SmCo}_5$  we use  $M_S = 851.91$  emu/cm<sup>3</sup>,  $A = 22 \times 10^{-7}$  erg/cm, and  $K = 1.7 \times 10^8$  erg/cm<sup>3</sup> [15]. For Fe we use  $M_S = 1711.78$  emu/cm<sup>3</sup>,  $A = 25 \times 10^{-7}$  erg/cm, and  $K = 4.8 \times 10^5$  erg/cm<sup>3</sup> [15]. For small core diameter ( $D = 3.5$  nm, 4.5 nm, and 7.5 nm)  $\text{SmCo}_5@Fe$  nanoparticles, we have used a small cell simulation size ( $d = 0.5$  nm) and for the 11 nm and 21 nm core diameter HSCS nanoparticles, we have used  $d = 1$  nm.

The strength of the core-shell exchange energy is a key issue and has been examined in recent reports. There are indications that a graded interface, separating the hard and soft phases of exchange coupled nanocomposites, may strengthen the effective exchange coupling and enhance the energy product [19–22].

We make the simplifying assumption of a sharp interface and a uniform core-shell exchange energy coupling. We use an effective exchange parameter  $A^*$ , which measures the interface exchange energy in units of the  $\text{SmCo}_5$  core exchange stiffness. We use  $A^* = 1$  for the present results. Furthermore, we assume that the uniaxial anisotropy energy density is uniform, within the core volume, and within the shell.

Throughout the paper, unless specified, we have selected the  $z = 0$  layer to show the magnetization and dipolar field patterns.  $\theta$  is the angle with the  $x$  axis, in the  $xy$  plane, and  $\varphi$  is the angle with the  $z$  axis.

## III. RESULTS AND DISCUSSIONS

The theoretical maximum value of the energy product is  $4\pi^2 M^2$  [10], and the saturation magnetization  $M$  of small core diameter HSCS nanoparticles increases rapidly with the shell thickness. Thus, one may think of choosing small core diameter HSCS nanoparticles with large values of the shell thickness, in order to optimize the energy product value.

This intuitive picture is valid to some extent. However, for a given value of the core diameter, there is an optimum value of the shell thickness ( $\delta^*$ ) beyond which it is no longer possible to

benefit from the increase in the saturation magnetization, and the value of the energy product drops. The value of the shell thickness must be such as to maximize the core-shell saturation magnetization, yet granting that the core and shell magnetizations be parallel to each other in the demagnetization quadrant, starting from  $H = 0$  up to the critical value of the external field strength  $H^*$  corresponding to the maximum energy product.

Achieving the theoretical maximum value of the energy product requires the HSCS nanoparticle magnetization  $M$  to be unchanged in the demagnetization quadrant and equal to the saturation value, starting at remanence ( $H = 0$ ) up to an external field strength of  $H_0^* = 2\pi M$  in the direction opposite to the magnetization [10]. Thus, the main goal is to ensure that the external field strength  $H_N$  required for the nucleation of magnetization reversal be larger than the  $2\pi M$  and that  $H^* = 2\pi M$ .

We have found that small core diameter  $\text{SmCo}_5@Fe$  nanoparticles are less vulnerable to the core-shell dipolar interaction effects, exhibit coherent reversal hysteresis loops, and may be tailored to achieve a large enhancement of the energy product.

Large diameter HSCS nanoparticles require thicker shells to achieve a significant percentage shell volume fraction to benefit from the large value of the shell magnetization. The large value of the core perimeter and the thicker shell thickness allow the nucleation of nonuniform shell magnetization patterns in the demagnetization quadrant. Thus, noncoherent reversal is favored, leading to reduction of the magnetization, in the demagnetization quadrant, and of the value of the energy product. We have found that for  $\text{SmCo}_5(D)@Fe(\delta)$  nanoparticles with diameter  $D$  ranging from 3.5 nm up to 11 nm, and Fe shell thickness up to 6 nm, the critical point  $H^*$  happens to be with magnetization at the saturation value and  $H^* \leq H_N$ .

For the  $\text{SmCo}_5(21 \text{ nm})@Fe(\delta)$  nanoparticles this is true only for Fe shell thicknesses smaller than 6 nm. For  $\delta \geq 6$  nm the critical field corresponds to a magnetic phase with reduced magnetization due to the magnetization drop produced by the shell vortex phase.

In Figs. 1(a)–1(c) we show typical magnetization patterns of  $\text{SmCo}_5(3.5 \text{ nm})@Fe(2.5 \text{ nm})$ ,  $\text{SmCo}_5(11 \text{ nm})@Fe(6.0 \text{ nm})$ , and  $\text{SmCo}_5(21 \text{ nm})@Fe(6.0 \text{ nm})$  nanoparticles, in the demagnetization quadrant. The dipolar field map of the 21 nm diameter core of the  $\text{SmCo}_5(21 \text{ nm})@Fe(6.0 \text{ nm})$  nanoparticle is shown in Fig. 1(d). The  $\text{SmCo}_5$  core is uniformly magnetized and represented schematically.

It is readily seen that the ferromagnetic interface energy prevails for the  $\text{SmCo}_5(3.5 \text{ nm})@Fe(2.5 \text{ nm})$  nanoparticle, and the dipolar field effects are largest for the 21 nm diameter core  $\text{SmCo}_5(21 \text{ nm})@Fe(6.0 \text{ nm})$  nanoparticle. At the critical field for maximum energy product,  $H = -10.31$  kOe ( $2\pi M = 10.31$  kG), the core and shell magnetizations of the  $\text{SmCo}_5(3.5 \text{ nm})@Fe(2.5 \text{ nm})$  nanoparticle are parallel, and the magnetization is equal to the saturation value.

The dipolar field of the 21 nm diameter  $\text{SmCo}_5$  core of the  $\text{SmCo}_5(21 \text{ nm})@Fe(6.0 \text{ nm})$  nanoparticle lies in the  $z = 0$  plane, and the  $x$  component varies from 6.5 kOe near the  $\theta = 0$  and  $\theta = \pi$  poles, to  $-3.2$  kOe at the  $\theta = \pi/2$  belt. The 11 nm core  $\text{SmCo}_5(11 \text{ nm})@Fe(6.0 \text{ nm})$  nanoparticle produces a similar dipolar field in the Fe shell. The magnetic patterns of  $\text{SmCo}_5(11 \text{ nm})@Fe(6.0 \text{ nm})$  and  $\text{SmCo}_5$

TABLE I.  $(BH)_{\text{max}}\text{-SmCo}_5(D)@Fe(\delta)$  core-shell nanoparticles.  $\delta^*$  is the optimum value of the Fe shell thickness, for each value of the  $\text{SmCo}_5$  core diameter, corresponding to the best core-shell composition.

Core diameter (D) (nm)	Fe( $\delta^*$ ) (nm)	$(BH)_{\text{max}}^*$ (MGOe)	Shell vol fraction (%)	Amplify factor
3.5 nm	2.5	106.30	93.0	3.72
4.5 nm	3.0	105.60	92.0	3.68
7.5 nm	4.0	100.48	88.7	3.50
11.0 nm	4.0	92.53	80.6	3.20
21.0 nm	4.0	74.00	62.0	2.60

(21 nm) $@Fe(6.0 \text{ nm})$  nanoparticles are shown for external field values of  $H = -5.35$  kOe and  $H = -12.5$  kOe and reveal the shell vortex phase.

In both cases, the shell displays a magnetization curling pattern, in a plane perpendicular to the core magnetization, and a component along the  $x$  direction that resembles the core dipolar field, in the shell region near the  $\text{SmCo}_5$  core poles ( $\theta = 0$  and  $\theta = \pi$ ). Notice that in both cases, away from the  $\text{SmCo}_5$  core poles ( $\theta = 0$  and  $\theta = \pi$ ), the curling magnetization at the shell corresponds to out of plane angle  $\varphi \approx 0$  (lower shell area, near  $\theta \approx -\pi/2$ ) and  $\varphi \approx \pi$  (upper shell area, near  $\theta \approx \pi/2$ ).

Furthermore, the larger shell perimeter, at the shell surface, of the  $\text{SmCo}_5(21 \text{ nm})@Fe(6.0 \text{ nm})$  nanoparticle, allows, in the  $\theta = \pi/2$  belt, the alignment of the shell magnetization with the core magnetization at the interface, and with the core dipolar field, at the shell surface. Figure 2 and Table I show a summary of our results for  $\text{SmCo}_5(D)@Fe(\delta)$  core-shell nanoparticles with  $\text{SmCo}_5$  core diameter ( $D$ ) ranging from 3.5 nm to 21 nm and Fe shell thicknesses ( $\delta$ ) up to 5 nm.

For any of the chosen core diameter values, as shown in Fig. 2, the energy product curve increases, as a function of the Fe shell thickness  $\delta$ , up to an optimum thickness value  $\delta^*$ . The optimum shell thickness value increases with core diameter size but saturates rapidly since the shell percentage volume fraction also saturates, as seen in Fig. 3.

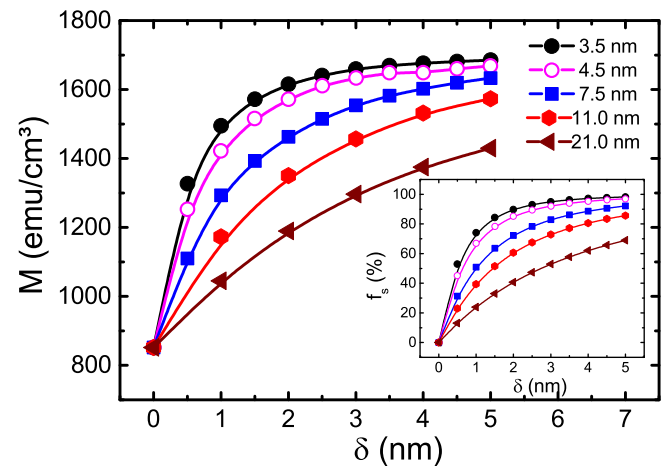


FIG. 3. Magnetization of  $\text{SmCo}_5(D)@Fe(\delta)$  core-shell nanoparticles, with core diameters  $D$  of 3.5, 4.5, 7.5, 11, and 21 nm, and Fe shells thicknesses  $\delta$  ranging from 0 to 5 nm. In the inset we show the percentage shell volume fraction.

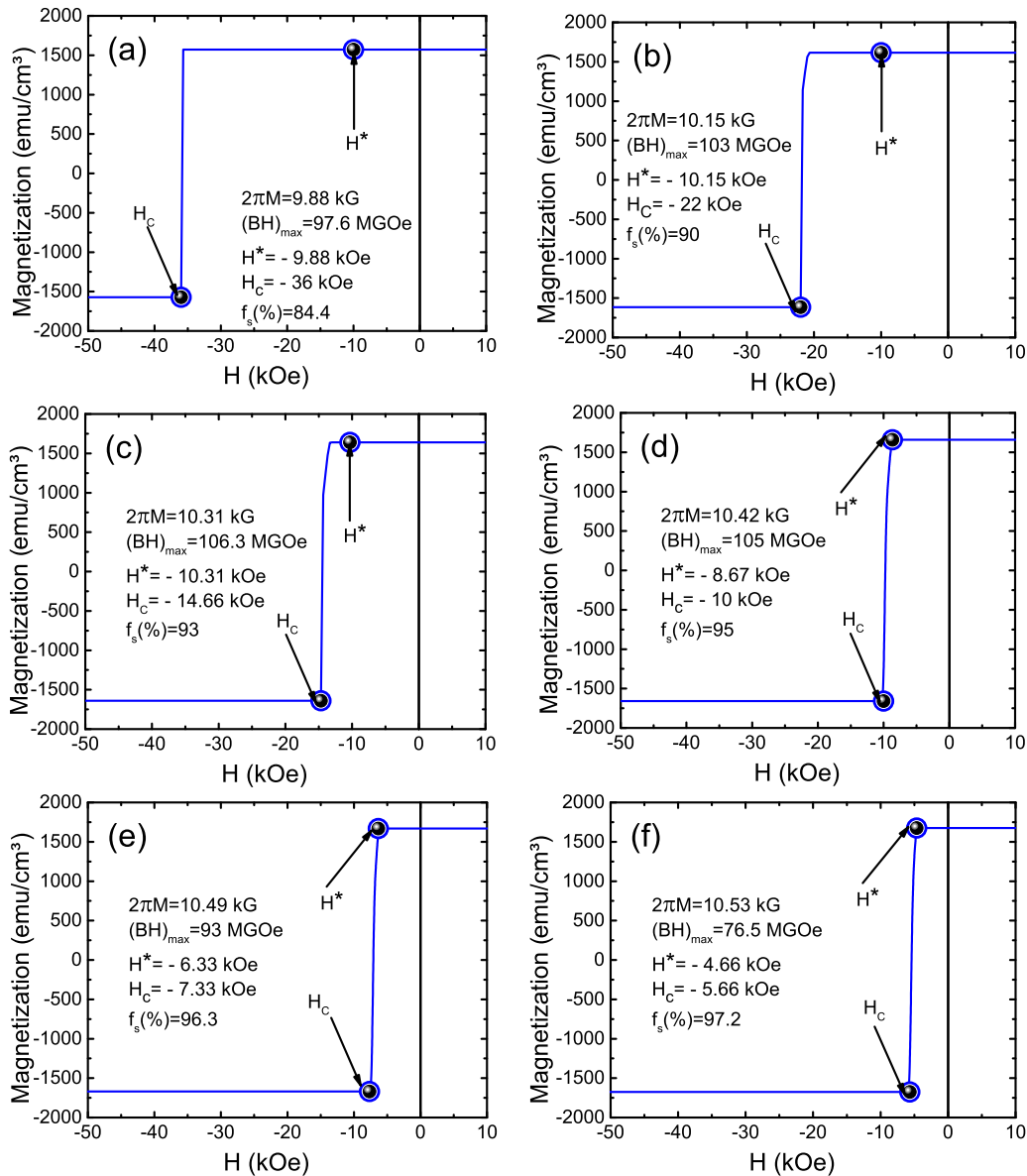


FIG. 4. Magnetization in the demagnetization quadrant of (a)  $\text{SmCo}_5(3.5 \text{ nm})@Fe(1.5 \text{ nm})$ , (b)  $\text{SmCo}_5(3.5 \text{ nm})@Fe(2.0 \text{ nm})$ , (c)  $\text{SmCo}_5(3.5 \text{ nm})@Fe(2.5 \text{ nm})$ , (d)  $\text{SmCo}_5(3.5 \text{ nm})@Fe(3.0 \text{ nm})$ , (e)  $\text{SmCo}_5(3.5 \text{ nm})@Fe(3.5 \text{ nm})$ , and (f)  $\text{SmCo}_5(3.5 \text{ nm})@Fe(4.0 \text{ nm})$  core-shell nanoparticles.

For  $\delta < \delta^*$  we have found that the external field strength for nucleation of reversal is larger than  $2\pi M$ . In this thickness range, for all chosen values of the  $\text{SmCo}_5$  core diameter, the energy product is equal to the theoretical maximum value,  $4\pi^2 M^2$ . This is shown in Fig. 2 for the  $D = 3.5 \text{ nm}$  diameter and for the  $D = 21 \text{ nm}$  diameter  $\text{SmCo}_5(D)@Fe(\delta)$  nanoparticles.

One advantage of small core diameter nanoparticles, as building blocks for high-energy product permanent magnet systems, is that the shell percentage volume fraction increases very rapidly with the shell thickness (see Fig. 3). As a result, as can be seen from Figs. 2 and 3, for a given shell thickness value, the  $3.5 \text{ nm}$  diameter  $\text{SmCo}_5$  core nanoparticle has larger values of  $M$ ,  $(BH)_{\text{max}}$ , and the percentage shell volume fraction.

Consider, for instance  $\delta = 1 \text{ nm}$  core-shell nanoparticles. The values of  $(BH)_{\text{max}}$ ,  $M$ , and the percentage shell volume fraction drop from  $88.17 \text{ MGOe}$ ,  $1494.6 \text{ emu/cm}^3$ , and  $74\%$ , for the  $3.5 \text{ nm}$  diameter  $\text{SmCo}_5$  core nanoparticle, down to  $42.82 \text{ MGOe}$ ,  $1045.1 \text{ emu/cm}^3$ , and  $24\%$  for the  $21 \text{ nm}$  diameter  $\text{SmCo}_5$  core nanoparticle. Thus, one may expect to achieve the best enhancement of the energy product using  $3.5 \text{ nm}$   $\text{SmCo}_5$  core nanoparticles.

As shown in Fig. 2, we have found that a  $3.5 \text{ nm}$  core diameter  $\text{SmCo}_5(3.5 \text{ nm})@Fe(\delta)$  nanoparticle, has an optimum shell thickness of  $\delta^* = 2.5 \text{ nm}$  and an energy product of  $106.3 \text{ MGOe}$ , which is  $3.7$  larger than that of the theoretical maximum value of the energy product ( $4\pi^2 M^2$ ) of the  $\text{SmCo}_5$  core ( $28.6 \text{ MGOe}$ ) and twice as large as that of  $\text{NdFeB}$  magnets [23]. The percentage shell volume fraction of the

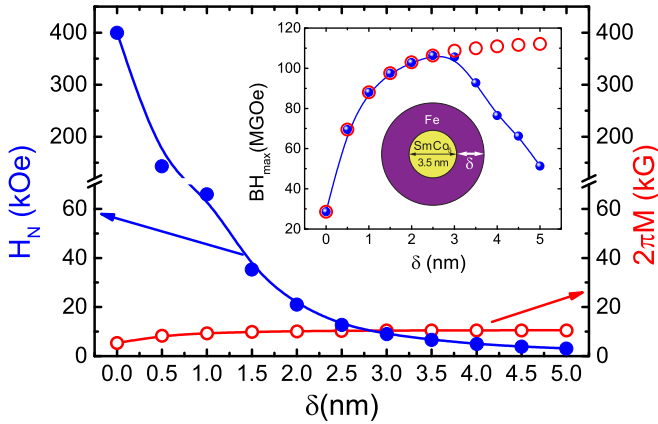


FIG. 5. Coercive field and  $2\pi M$  of  $\text{SmCo}_5(3.5 \text{ nm})@Fe(\delta \text{ nm})$  core-shell nanoparticles (the continuous lines are just a guide to the eyes). The inset shows the curves for the energy product  $(BH)_{max}$  (full symbol curve) and the theoretical maximum energy product  $4\pi^2 M^2$  (open symbol curve).

$\text{SmCo}_5(3.5 \text{ nm})@Fe(2.5 \text{ nm})$  nanoparticle is 93% and the saturation magnetization is  $1641 \text{ emu/cm}^3$ . The hysteresis loop is square with a coercivity of  $H_C = 14.66 \text{ kOe}$ . The external field strength for theoretical maximum energy product value is  $H_0^* = 2\pi M = 10.3 \text{ kOe}$ . Therefore  $H_C > H_0^*$  and, for external field strength  $H \leq H_0^*$ , in demagnetization quadrant, the magnetization is equal to the saturation magnetization.

In order to reach a percentage shell volume fraction of 93%, a 21 nm core diameter  $\text{SmCo}_5(21 \text{ nm})@Fe(\delta \text{ nm})$  HSCS nanoparticle requires an Fe shell thickness of  $\delta = 15 \text{ nm}$ . This would lead to a rather small energy product value. As we show below, we have found that even for a much thinner Fe shell, with thickness of  $\delta = 8 \text{ nm}$ , the energy product of the  $\text{SmCo}_5(21 \text{ nm})@Fe(8 \text{ nm})$  is 16 MGOe, which is smaller than that of the  $\text{SmCo}_5$  core.

We show in Fig. 4 the magnetization curves in the demagnetization quadrant of small core diameter  $\text{SmCo}_5(3.5 \text{ nm})@Fe(\delta)$  nanoparticles, for values of the Fe shell thickness of  $\delta = 1.5 \text{ nm}, 2.0 \text{ nm}, 2.5 \text{ nm}, 3.0 \text{ nm}, 3.5 \text{ nm},$  and  $4 \text{ nm}$ . The nanoparticles exhibit coherent reversal,  $H_N = H_C$ , and the coercive field  $H_C$  ranges from 36 kOe, for the  $\text{SmCo}_5(3.5 \text{ nm})@Fe(1.5 \text{ nm})$  nanoparticle, down to 5.66 kOe for the  $\text{SmCo}_5(3.5 \text{ nm})@Fe(4 \text{ nm})$  nanoparticle. The value of the critical field for theoretical maximum energy product,  $H_0^* = 2\pi M$ , increases from 9.88 kG for the  $\text{SmCo}_5(3.5 \text{ nm})@Fe(1.5 \text{ nm})$  nanoparticle up to 10.53 kG for the  $\text{SmCo}_5(3.5 \text{ nm})@Fe(4 \text{ nm})$  nanoparticle. For Fe shell thicknesses smaller or equal to 2.5 nm, we have found that  $H_0^* < H_C$ , and the energy product is equal to the theoretical maximum value. For  $\delta \geq 3 \text{ nm}$ , we have found that  $H_0^* > H_C$ . In this thickness range, the maximum energy product corresponds to the external field strength value ( $H^*$ ) immediately before the value required for magnetization reversal ( $H^* \approx H_C$ ).

Our results for 3.5 nm  $\text{SmCo}_5$  core diameter nanoparticles,  $\text{SmCo}_5(3.5 \text{ nm})@Fe(\delta)$ , for Fe shell thicknesses ranging from  $\delta = 0.5 \text{ nm}$  to  $\delta = 5 \text{ nm}$ , are summarized in Fig. 5. We show the impact of the Fe shell thickness  $\delta$  on the reduction of the external field strength for nucleation of reversal,  $H_N$ , and on the value of the critical field ( $2\pi M$ ) for the theoretical maximum value of the energy product.

For these nanoparticles, the reversal is sharp and the external field strength for nucleation of reversal ( $H_N$ ) is equal to the coercive field ( $H_C$ ). In the inset, we show the value of the energy product, calculated using the present theoretical model, and the theoretical maximum value of the energy product. Notice that for values of  $\delta$  for which  $H_N$  is larger than  $2\pi M$ , the energy product is equal to the theoretical maximum value  $4\pi^2 M^2$ . For  $\delta \geq 3.0 \text{ nm}$  the reversal field turns smaller than  $2\pi M$  and the energy product is smaller than the theoretical maximum value. In this thickness range the value of  $(BH)_{max}$  decreases as the Fe thickness  $\delta$  increases.

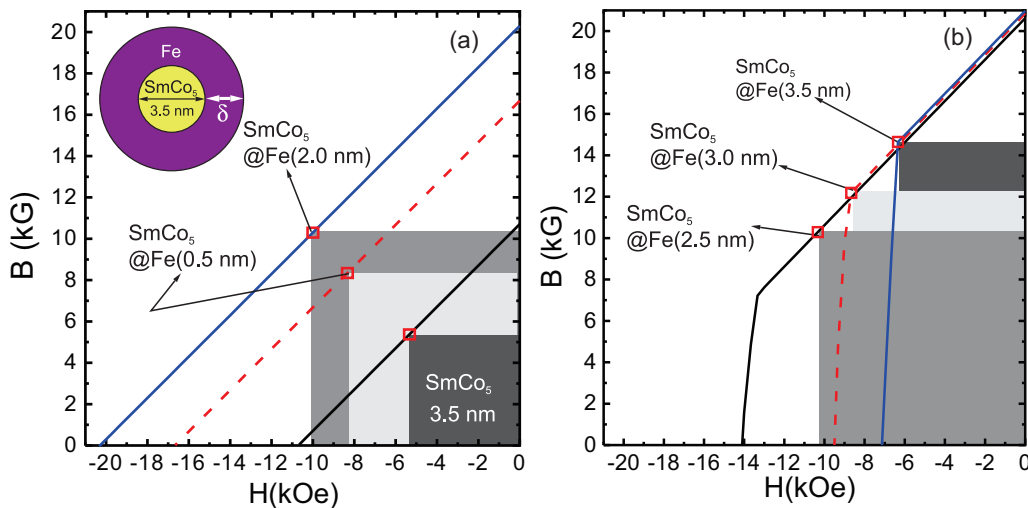


FIG. 6. Demagnetization curves of core-shell nanoparticles for (a) isolated  $\text{SmCo}_5(3.5 \text{ nm})$  core,  $\text{SmCo}_5(3.5 \text{ nm})@Fe(0.5 \text{ nm})$ , and  $\text{SmCo}_5(3.5 \text{ nm})@Fe(2.0 \text{ nm})$  core-shell nanoparticles and (b)  $\text{SmCo}_5(3.5 \text{ nm})@Fe(2.5 \text{ nm})$ ,  $\text{SmCo}_5(3.5 \text{ nm})@Fe(3.0 \text{ nm})$ , and  $\text{SmCo}_5(3.5 \text{ nm})@Fe(3.5 \text{ nm})$  core-shell nanoparticles. The squares in (a) and rectangles in (b) indicate the areas corresponding to the high-energy product  $(BH)_{max}$ .

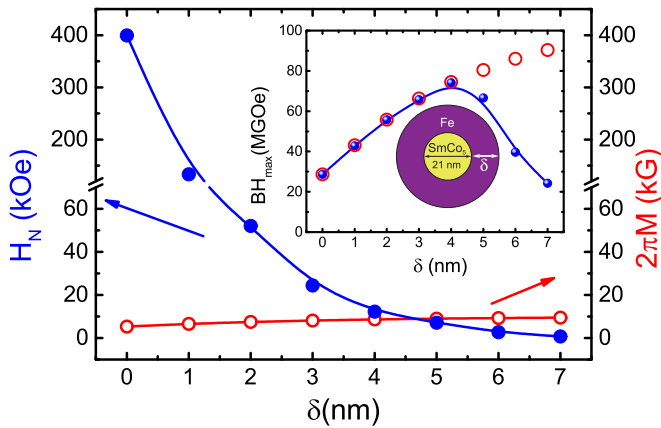


FIG. 7. Nucleation field and  $2\pi M$  of  $\text{SmCo}_5(21 \text{ nm})@Fe(\delta \text{ nm})$  core-shell nanoparticles. The inset shows the curves for the energy product  $(BH)_{\max}$  (full symbol curve) and the theoretical maximum energy product  $4\pi^2 M^2$  (open symbol curve).

In Fig. 6 we show  $B(H)$  in the demagnetization quadrant for the 3.5 nm diameter  $\text{SmCo}_5$  core, and  $\text{SmCo}_5(3.5 \text{ nm})@Fe(\delta)$  nanoparticles, for Fe shell thicknesses from  $\delta = 0.5 \text{ nm}$ , to  $\delta = 3.5 \text{ nm}$ . As seen in Fig. 6(a), the  $B(H)$  curves for the  $\text{SmCo}_5$  core, and for  $\delta = 0.5 \text{ nm}$  and  $\delta = 2.0 \text{ nm}$   $\text{SmCo}_5(3.5 \text{ nm})@Fe(\delta)$  nanoparticles, are straight lines, from  $B = 4\pi M$ , at  $H = 0$ , to  $B = 0$ , at  $H = -4\pi M$ . In these three cases  $2\pi M \approx 5.4 \text{ kOe}$ ,  $8.3 \text{ kOe}$ , and  $10.2 \text{ kOe}$ , the coercive fields are  $399 \text{ kOe}$ ,  $147 \text{ kOe}$ , and  $22 \text{ kOe}$ , and the energy product is equal to the theoretical maximum value ( $4\pi^2 M^2$ ).

In Fig. 6(b) we show the  $B(H)$  curves for  $\delta = 2.5 \text{ nm}$ ,  $\delta = 3 \text{ nm}$ , and  $\delta = 3.5 \text{ nm}$  thick Fe shells. The values of  $2\pi M$  are a nearly equal,  $2\pi M \approx 10.31 \text{ kOe}$ ,  $10.42 \text{ kOe}$ , and  $10.49 \text{ kOe}$ . The  $\text{SmCo}_5(3.5 \text{ nm})@Fe(2.5 \text{ nm})$  nanoparticle has a coercive field of  $14.66 \text{ kOe}$ , which is larger than  $2\pi M$ , and an energy product equal to the theoretical maximum value. The 3 nm and 3.5 nm thick Fe shells nanoparticles have coercivities of  $10 \text{ kOe}$  and  $7.3 \text{ kOe}$ , which are smaller than the corresponding values of  $2\pi M$ . For these nanoparticles the energy product is smaller than the theoretical maximum value.

We have found that the 21 nm core diameter  $\text{SmCo}_5(21 \text{ nm})@Fe(\delta)$  nanoparticle has an optimum shell thickness of  $\delta^* = 4 \text{ nm}$ . The  $\text{SmCo}_5(21 \text{ nm})@Fe(4 \text{ nm})$  has an energy product of  $74 \text{ MGOe}$ , which is 2.58 larger than that of the theoretical maximum value of the energy product ( $4\pi^2 M^2$ ) of the  $\text{SmCo}_5$  core ( $28.6 \text{ MGOe}$ ). The percentage shell volume fraction is 62% and the saturation magnetization is  $1378 \text{ emu/cm}^3$ . The external field strength for the nucleation of reversal is  $12.29 \text{ kOe}$ , while the maximum energy product corresponds to an external field strength of  $H^* = 8.63 \text{ kOe}$ .

We have considered  $\text{SmCo}_5(21 \text{ nm})@Fe(\delta)$  nanoparticles with Fe shell thicknesses from 1 nm up to 8 nm. In Fig. 7 we show the impact of the Fe shell thickness  $\delta$  on the reduction of the external field strength for nucleation of reversal,  $H_N$ , and on the value of the  $2\pi M$  corresponding to the saturation magnetization. In the inset, we show the value of the energy product, calculated using the present theoretical model, and the theoretical maximum value of the energy product. Notice that for values of  $\delta$  for which  $H_N$  is larger than  $2\pi M$ , the energy

product is equal to the theoretical maximum value  $4\pi^2 M^2$ . For  $\delta \geq 5.0 \text{ nm}$  the reversal field turns smaller than  $2\pi M$  and the energy product is smaller than the theoretical maximum value.

As shown in Fig. 8,  $\text{SmCo}_5(21 \text{ nm})@Fe(\delta)$  nanoparticles do not exhibit coherent reversal, and for  $\delta \leq \delta^*$  the points in the demagnetization quadrant corresponding to the maximum energy product have the magnetization equal to the saturation value. In addition, except for small shell thickness ( $\delta = 1 \text{ nm}$  and  $\delta = 2 \text{ nm}$ ) nanoparticles, the magnetization reversal requires a wide external field interval and exhibits a compensation point (where  $M = 0$ ). At the compensation point the net shell magnetization cancels the core magnetization. In all cases the core switches at large external field values, ranging from  $H = -160 \text{ kOe}$  to  $-83 \text{ kOe}$ , and the magnetization variation is proportional to the core percentage volume fraction.

For  $\delta > \delta^*$  the point for maximum energy product corresponds to a magnetic phase in which the Fe shell magnetization is no longer parallel to the  $\text{SmCo}_5$  core magnetization. For instance, for Fe shell thicknesses of 6 nm, the critical field is  $H^* = -3.5 \text{ kOe}$ , the nucleation field is  $H_N = -3.0 \text{ kOe}$ , and, at the maximum energy product point, the magnetization has dropped to 80% of the saturation value. For Fe shell thickness of 8 nm, the critical field is  $H^* = -2.0 \text{ kOe}$ , the nucleation field is  $H_N = 0.0 \text{ kOe}$ , and, at the maximum energy product point, the magnetization has dropped to 50% of the saturation value.

The 21 nm diameter, 8 nm Fe shell thickness  $\text{SmCo}_5(21 \text{ nm})@Fe(8 \text{ nm})$  nanoparticle has a percentage shell volume fraction of 82%, a saturation magnetization of  $1541 \text{ emu/cm}^3$ , which is 81% larger than the saturation magnetization of the  $\text{SmCo}_5$  core. In optimized conditions, with the  $\text{SmCo}_5$  core exchange coupled to the Fe shell in the demagnetization quadrant, this large value of magnetization would lead to an energy product 3.27 times larger than that of the  $\text{SmCo}_5$  core. However, the energy product of the  $\text{SmCo}_5(21 \text{ nm})@Fe(8 \text{ nm})$  nanoparticle is  $16 \text{ MGOe}$ , which is smaller than the theoretical maximum value of the energy product of the  $\text{SmCo}_5$  core. This considerable drop in the energy product is associated with the nucleation of the shell vortex phase in the demagnetization quadrant, as discussed below.

Notice that there are relevant reductions of the external field strength and the magnetization at the critical point for maximum energy product. The external field strength ( $2 \text{ kOe}$ ) is much smaller than  $2\pi M = 9.7 \text{ kG}$  (required for the theoretical maximum energy product value). The magnetization is  $778 \text{ emu/cm}^3$  which is 50% of the saturation value.

There is a relevant impact of both the  $\text{SmCo}_5$  core diameter value and the Fe shell thickness value on the energy product. For instance, we have found that the 21 nm  $\text{SmCo}_5$  core diameter, 6 nm Fe shell thickness  $\text{SmCo}_5(21 \text{ nm})@Fe(6 \text{ nm})$  nanoparticle has a shell volume fraction of 74%, a saturation magnetization of  $1460 \text{ emu/cm}^3$ , and an energy product of  $39.6 \text{ MGOe}$ , as shown in Fig. 9. We have also found that, with the same Fe shell thickness, the 11 nm core diameter  $\text{SmCo}_5(11 \text{ nm})@Fe(6 \text{ nm})$  nanoparticle has a larger shell volume fraction of 85.06%, a saturation magnetization of  $1572.8 \text{ emu/cm}^3$ , and an energy product of  $46.31 \text{ MGOe}$ . The energy product of the  $\text{SmCo}_5(11 \text{ nm})@Fe(6 \text{ nm})$  nanoparticle is 74% larger. Judging from the values of the saturation magnetizations, and the theoretical maximum value of the energy product, given

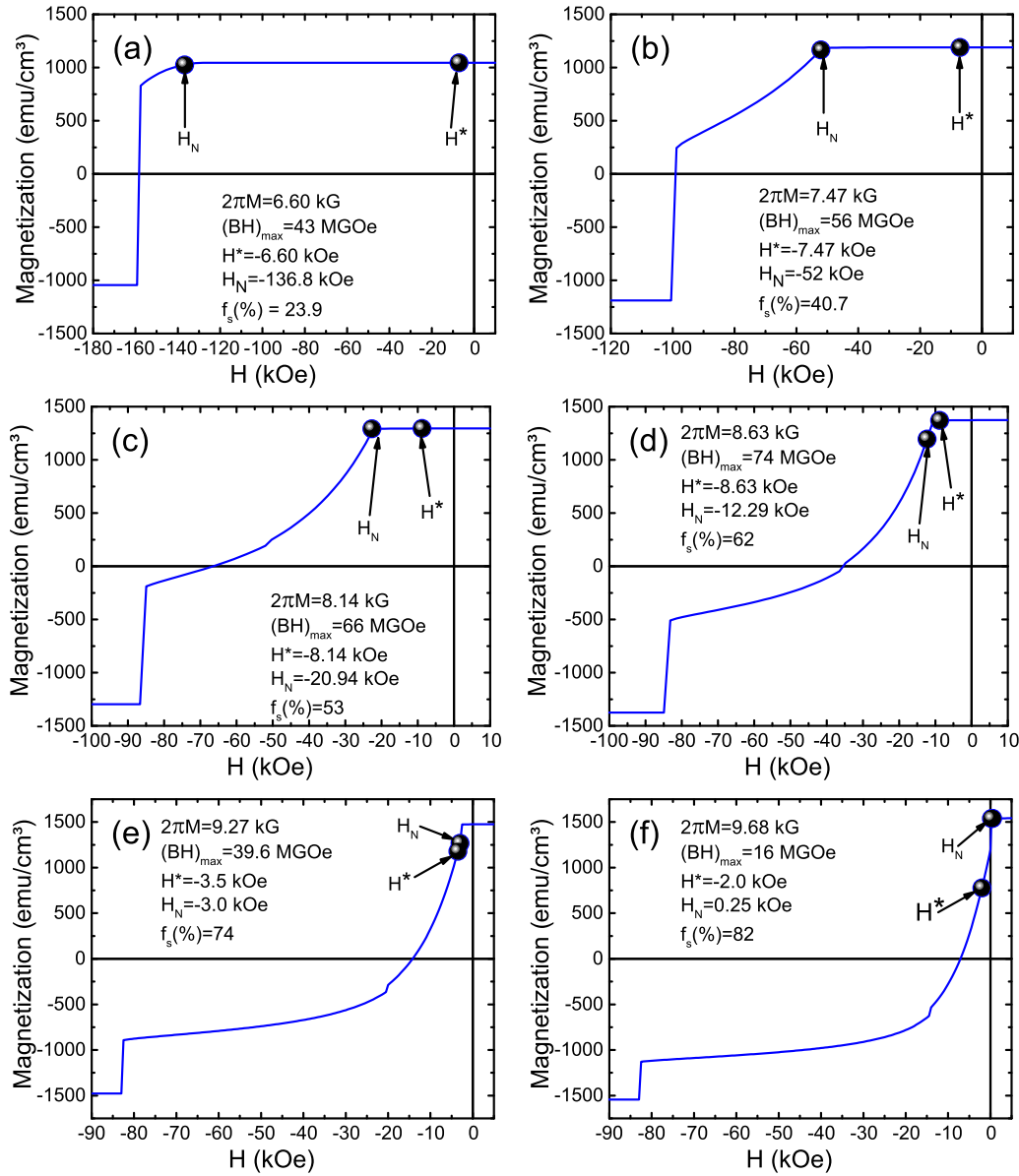


FIG. 8. Magnetization in the demagnetization quadrant of (a) SmCo<sub>5</sub>(21 nm)@Fe(1.0 nm), (b) SmCo<sub>5</sub>(21 nm)@Fe(2.0 nm), (c) SmCo<sub>5</sub>(21 nm)@Fe(3.0 nm), (d) SmCo<sub>5</sub>(21 nm)@Fe(4.0 nm), (e) SmCo<sub>5</sub>(21 nm)@Fe(6.0 nm), and (f) SmCo<sub>5</sub>(21 nm)@Fe(8.0 nm) core-shell nanoparticles.

by  $4\pi^2 M^2$ , one would expect that the energy product of the SmCo<sub>5</sub>(11 nm)@Fe(6 nm) nanoparticle would be only 14% larger than that of the SmCo<sub>5</sub>(21 nm)@Fe(6 nm) nanoparticle. The large difference in the energy product of the SmCo<sub>5</sub>(11 nm)@Fe(6 nm) and the SmCo<sub>5</sub>(21 nm)@Fe(6 nm) nanoparticles is due to the magnetic phases in the demagnetization quadrant corresponding to the point of maximum energy product. The larger core diameter of the SmCo<sub>5</sub>(21 nm)@Fe(6 nm) nanoparticle allows more room for the relaxation of the shell magnetization, starting at the core surface up to the shell surface, allowing the nucleation of the shell vortex phase.

In the shell vortex state, the shell displays a curling magnetization pattern, in a plane perpendicular to the core magnetization, and a component along the  $x$  direction that resembles the core dipolar field near the poles of the core. At the  $\theta \approx \pi/2$  belt, the  $x$  component of the shell magnetization

relaxes from alignment with the core magnetization at core-shell interface to an angle at the shell surface that varies along the demagnetization curve.

In Fig. 9(a) we show the demagnetization curves of the SmCo<sub>5</sub>(11 nm)@Fe(6 nm) and SmCo<sub>5</sub>(21 nm)@Fe(6 nm) nanoparticles. In Fig. 9(b) we show details of the shell vortex state of the SmCo<sub>5</sub>(21 nm)@Fe(6 nm) nanoparticle at selected points in the demagnetization curve. Notice that Fig. 9(a) displays global data of the SmCo<sub>5</sub>(11 nm)@Fe(6 nm) and SmCo<sub>5</sub>(21 nm)@Fe(6 nm) nanoparticles, while Fig. 9(b) shows information regarding the local magnetization pattern of the SmCo<sub>5</sub>(21 nm)@Fe(6 nm) nanoparticle.

The panels in Fig. 9(b) shows the curling magnetization pattern at the  $yz$  plane, and the color barcode shows  $S_x$ , the  $x$  component of the shell magnetization, in units of the Fe saturation magnetization, in the shell area, or the SmCo<sub>5</sub>

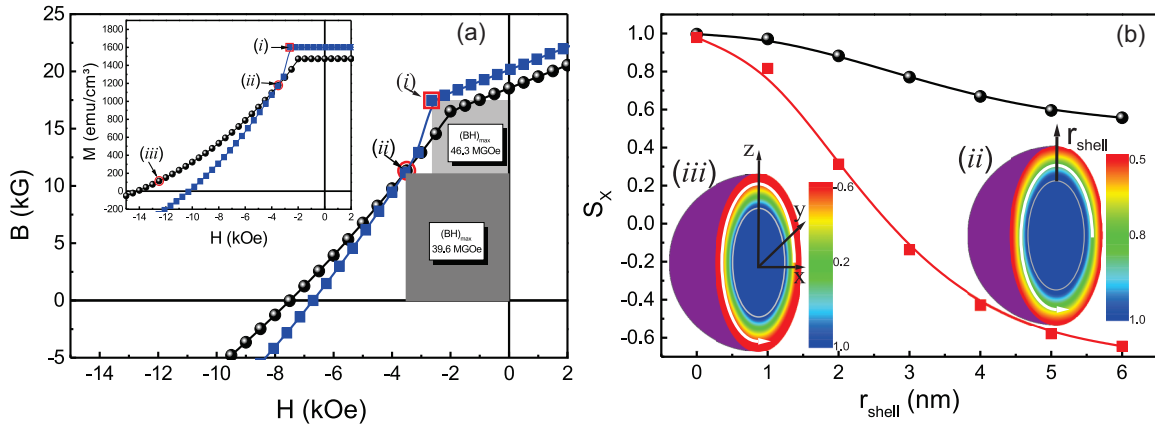


FIG. 9. (a) Demagnetization curves, of  $\text{SmCo}_5(21 \text{ nm})@Fe(6 \text{ nm})$  (circle symbols curve) and  $\text{SmCo}_5(11 \text{ nm})@Fe(6 \text{ nm})$  (square symbols curve) nanoparticles. Selected points (i) and (ii) indicate the points of maximum energy product of the  $\text{SmCo}_5(11 \text{ nm})@Fe(6 \text{ nm})$  and  $\text{SmCo}_5(21 \text{ nm})@Fe(6 \text{ nm})$  nanoparticles, and (iii) indicates a point in the demagnetization of the  $\text{SmCo}_5(21 \text{ nm})@Fe(6 \text{ nm})$  nanoparticle for  $H = -12.5 \text{ kOe}$ . The panels in (b) show the shell vortex phase magnetic pattern at selected points (ii), for  $H = -3.5 \text{ kOe}$  (circle symbols curve), and (iii), for  $H = -12.5 \text{ kOe}$  (square symbols curve), in the demagnetization curve of the  $\text{SmCo}_5(21 \text{ nm})@Fe(6 \text{ nm})$  nanoparticle.  $S_x$  is the  $x$  component of the shell magnetization, in units of the Fe saturation magnetization, along the radial direction within the  $\theta \approx \pi/2$  ( $0 < \varphi < 2\pi$ ) belt, from the shell interface layer, for  $r_{\text{shell}} = 1 \text{ nm}$ , to the nanoparticle's surface, for  $r_{\text{shell}} = 6 \text{ nm}$ . For comparison, we also show, for  $r_{\text{shell}} = 0$ , the  $x$  component of the core magnetization, in units of the  $\text{SmCo}_5$  saturation magnetization.

magnetization in the central area, corresponding to the core. Notice that in the core area,  $S_x = 1$ , while in the shell area  $S_x$  relaxes from near alignment with the core magnetization at the core-shell interface, to a value at the shell surface that is determined by the external field value.

As seen in Fig. 9(a), the interface exchange energy is favored in the  $\text{SmCo}_5(11 \text{ nm})@Fe(6 \text{ nm})$  nanoparticle due to its smaller core diameter. The point of maximum energy product,  $H = -2.65 \text{ kOe}$ , corresponds to the shell exchange coupled to the core and the magnetization equal to the saturation magnetization value ( $1601.8 \text{ emu/cm}^3$ ).

In the case of the  $\text{SmCo}_5(21 \text{ nm})@Fe(6 \text{ nm})$  nanoparticle, the point of maximum energy product,  $H = -3.5 \text{ kOe}$ , corresponds to partial alignment of the core and shell magnetizations. The magnetization is  $1178.6 \text{ emu/cm}^3$ . There is a 20% drop in the magnetization compared to the saturation value ( $1474.6 \text{ emu/cm}^3$ ).

As shown in Fig. 9(b), at the point of maximum energy product, the shell magnetization, at the  $yz$  plane, is parallel to the core magnetization, at the core-shell interface, and twists to a  $\pi/3$  direction at the shell surface. Therefore, only a fraction of the Fe shell magnetization adds to the core magnetization leading to a modest enhancement of the energy product. Furthermore, as shown in Fig. 9(a), the nucleation of reversal occurs for an external field  $H_N = -3.0 \text{ kOe}$  and the external field for energy product maximum ( $H^* = -3.5 \text{ kOe}$ ) is much smaller than  $2\pi M = 9.27 \text{ kG}$  (required for the theoretical maximum energy product value). The magnetization is  $1179.9 \text{ emu/cm}^3$  which is 80% of the saturation value. Proceeding further along the demagnetization curve of the  $\text{SmCo}_5(21 \text{ nm})@Fe(6 \text{ nm})$  nanoparticle, as shown in Fig. 9(a), at the external field value  $H = -12.5 \text{ kOe}$ , the magnetization is  $114.16 \text{ emu/cm}^3$ , corresponding to only 8% of the saturation value.

As shown in Fig. 9(b), the large magnetization drop corresponds to a new profile of the shell vortex phase. At the

$\theta \approx \pi/2$  belt, the shell magnetization is nearly parallel to the core magnetization, at the core-shell interface, and twists to almost the opposite direction at the shell surface. The magnetization reversal proceeds via a gradual change in the shell vortex phase, in a wide field interval, from  $-3 \text{ kOe}$  to  $-83.5 \text{ kOe}$ , where the  $\text{SmCo}_5$  core switches [see Fig. 8(e)].

This is also the mechanism for magnetization reversal of the  $\text{SmCo}_5(21 \text{ nm})@Fe(8 \text{ nm})$  nanoparticle, as shown in Fig. 10. In this case, due to the thicker Fe shell, the reversal process occurs in a wider external field interval. The nucleation of reversal occurs at a positive external field,  $H = 0.25 \text{ kOe}$ , and the reversal occurs at  $H = -83 \text{ kOe}$  when the  $\text{SmCo}_5$  core switches [see Fig. 8(f)].

In Fig. 10 we show the shell magnetic pattern in the  $z = 0$  ( $xy$  plane) and  $x = 0$  ( $yz$  plane) layers for two values of the external field in the demagnetization curve of the  $\text{SmCo}_5(21 \text{ nm})@Fe(8 \text{ nm})$  nanoparticle. The  $yz$  plane panels allow a clear visualization of the shell magnetization curling and the relaxation of the shell magnetization from the core-shell interface up to the shell surface. The  $\text{SmCo}_5$  is uniformly magnetized and is represented schematically. The  $\text{SmCo}_5(21 \text{ nm})@Fe(8 \text{ nm})$  nanoparticle shell vortex phase forms for  $H = 0.25 \text{ kOe}$ , and for  $H = -2.67 \text{ kOe}$ , the shell vortex phase has a profile similar to that found at a much larger external field value ( $-12.5 \text{ kOe}$ ) in the  $\text{SmCo}_5(21 \text{ nm})@Fe(6.0 \text{ nm})$  nanoparticle (see Fig. 1).

As seen in Fig. 10(a), for  $H = -2.67 \text{ kOe}$ , the shell magnetization curling spreads over an approximately  $\pi$  wide belt centered at  $\theta = \pi/2$ . Figure 10(b) shows that the shell magnetization is almost parallel to the core magnetization at the core-shell interface and twists to a nearly perpendicular direction at the shell surface. The shell vortex phase leads to a reduction of the  $\text{SmCo}_5(21 \text{ nm})@Fe(8 \text{ nm})$  nanoparticle magnetization to  $652 \text{ emu/cm}^3$  (42% of the saturation value).

For  $H = -14.2 \text{ kOe}$  most of the shell volume is opposite to the core magnetization and the magnetization is

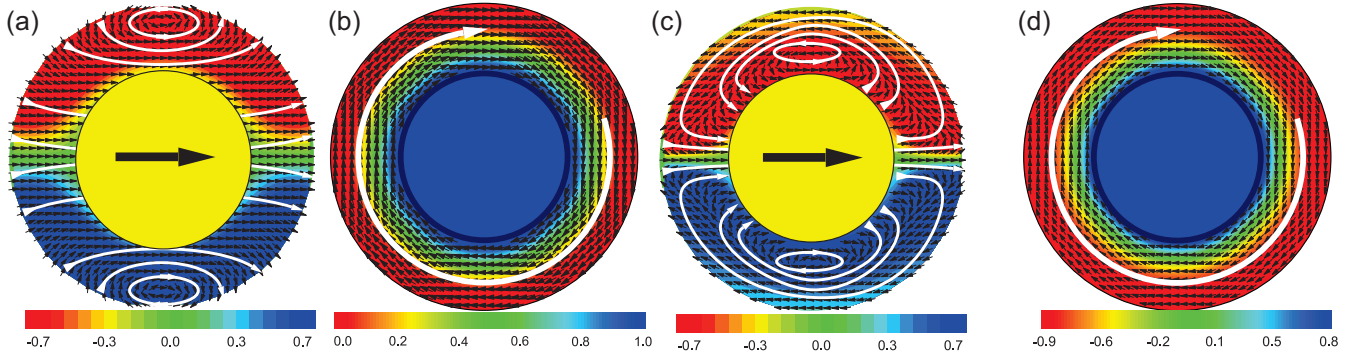


FIG. 10. Shell vortex phase patterns of a  $\text{SmCo}_5(21 \text{ nm})@Fe(8.0 \text{ nm})$  nanoparticle, for external field of  $-2.67 \text{ kOe}$  in the  $xy$  plane (a) and  $yz$  plane (b), and for external field of  $-14.2 \text{ kOe}$  in the  $xy$  plane (c) and  $yz$  plane (d). The color barcodes show the out-of-plane magnetization component in units of the  $\text{SmCo}_5$  (Fe) saturation magnetization in the core (shell).

$-542 \text{ emu/cm}^3$ . The shell vortex phase has a rather different magnetization profile, starting nearly aligned with the core at the core-shell interface, to the opposite direction in the shell surface.

The compensation points in the demagnetization curves of  $\text{SmCo}_5(21 \text{ nm})@Fe(6.0 \text{ nm})$  and  $\text{SmCo}_5(21 \text{ nm})@Fe(8.0 \text{ nm})$  nanoparticles reflect the external field effects on the gradual change in the shell vortex phase profile in the demagnetization quadrant. The shell vortex phase forms with a partial alignment of the  $x$  component with the core magnetization at small external field values and evolves to nearly the opposite direction along the demagnetization curve, as discussed in Fig. 9(b) for the  $\text{SmCo}_5(21 \text{ nm})@Fe(6.0 \text{ nm})$  nanoparticle. We may anticipate larger field effects in the  $8 \text{ nm}$  thick Fe shell nanoparticle.

Compared to the  $\text{SmCo}_5(21 \text{ nm})@Fe(6.0 \text{ nm})$  nanoparticle, the external field effects on the shell vortex profile of the  $\text{SmCo}_5(21 \text{ nm})@Fe(6.0 \text{ nm})$  nanoparticle are much stronger. The compensation points for the  $\text{SmCo}_5(21 \text{ nm})@Fe(6.0 \text{ nm})$  and  $\text{SmCo}_5(21 \text{ nm})@Fe(8.0 \text{ nm})$  nanoparticles are  $H = -14.3 \text{ kOe}$  and  $H = -7.0 \text{ kOe}$ .

The magnetic parameters of  $\text{SmCo}_5$  and Fe favor the formation of the shell vortex phase in  $\text{SmCo}_5@Fe$  spherical

core-shell nanoparticles. The values of the exchange stiffness are almost equal, while there is a large difference in the anisotropy density, favoring phases in which the core is uniformly magnetized.

Furthermore, the spherical core-shell structure enhances the core dipolar field effects in the shell magnetic pattern and disfavors the shell dipolar field effects in the core magnetic pattern. In other words, the impact of the core dipolar field in the shell magnetic pattern is stronger than that of the shell dipolar field in the core magnetic pattern.

Although having a magnetization of the order of half of the Fe magnetization, the  $\text{SmCo}_5$  core dipolar field produces nonuniform magnetization patterns in the Fe shell. The  $\text{SmCo}_5$  core dipolar field in the Fe shell is of the order of a few kOe, and the Fe shell anisotropy field is  $0.55 \text{ kOe}$ . Due to the large magnetization of the Fe shell, the core-shell dipolar energy overcomes the anisotropy energy barrier, favoring the nucleation of the shell vortex phase.

On the other hand, for all nanoparticles in the present study, we have found that the strength of the Fe shell dipolar field in the  $\text{SmCo}_5$  core is much smaller than the  $\text{SmCo}_5$  anisotropy field ( $\approx 400 \text{ kOe}$ ). Furthermore, the small value of the  $\text{SmCo}_5$  core magnetization turns the core-shell dipolar energy density

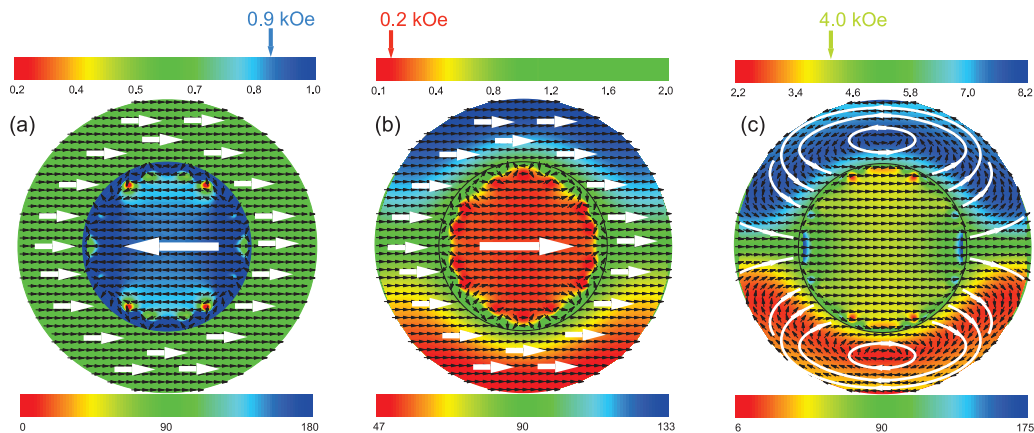


FIG. 11. The shell magnetization pattern and the dipolar field produced by the  $Fe(8 \text{ nm})$  shell in the  $\text{SmCo}_5(21 \text{ nm})$  core of the  $\text{SmCo}_5(21 \text{ nm})@Fe(8.0 \text{ nm})$  nanoparticle, for (a)  $H = 1 \text{ kOe}$ , (b)  $H = 0.25 \text{ kOe}$ , and (c)  $H = -7 \text{ kOe}$ . The bottom color barcodes show the out of plane angle  $\varphi$  of the shell magnetization. The top color barcodes show the intensity of the  $Fe(8.0 \text{ nm})$  shell dipolar field in the  $\text{SmCo}_5(21 \text{ nm})$  core.

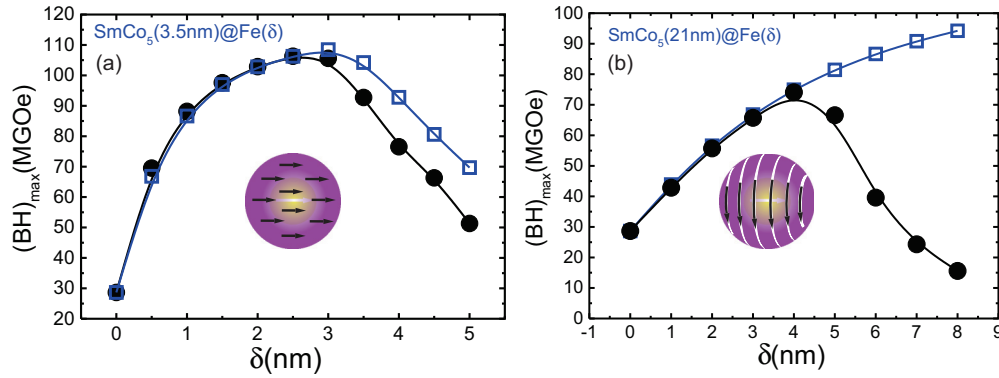


FIG. 12.  $(BH)_{\max}$  of (a)  $\text{SmCo}_5(3.5\text{ nm})@Fe(\delta)$  core-shell nanoparticles, and Fe shells thicknesses ( $\delta$ ) ranging from 0 to 5 nm, and (b)  $\text{SmCo}_5(21\text{ nm})@Fe(\delta)$  core-shell nanoparticles, and Fe shells thicknesses ( $\delta$ ) ranging from 0 to 8 nm. The curve with filled symbols corresponds to the present theoretical model, and the curve with open symbols corresponds to the average model approximation ( $\langle BH \rangle_{\max}$ ), which does not include the core-shell dipolar interaction.

much smaller than the anisotropy energy density in the  $\text{SmCo}_5$  core, favoring the stability of the core uniform magnetization phase.

Figure 11 shows the shell magnetization pattern and the shell dipolar field in the core, in selected points of the demagnetization curve of the  $\text{SmCo}_5(21\text{ nm})@Fe(8.0\text{ nm})$  nanoparticle. Notice that the shell dipolar field in the core has modest intensity, as compared to the core anisotropy field.

For an external field  $H = 1\text{ kOe}$ , with the Fe shell magnetization uniform ( $S_x = 1$  and  $\varphi = \pi/2$ ), as shown in Fig. 10(a), the Fe(8 nm) shell dipolar field in the  $\text{SmCo}_5(21\text{ nm})$  core is opposite to the direction of the core magnetization. In most of the core volume the shell dipolar field is of the order of 0.9 kOe.

Interestingly, at the nucleation of the shell vortex phase, for an external field of 0.25 kOe, as shown in Fig. 10(b), the shell dipolar field in the core switches to the direction of the core magnetization. The shell vortex phase covers a  $\pi/2$  wide belt centered at  $\theta = \pi/2$ . In most of the core, except for the regions near the poles at  $\theta = 0$  and  $\theta = \pi$ , the shell dipolar field is  $\approx 0.2\text{ kOe}$ .

Proceeding further along the demagnetization curve, at the compensation point, for an external field of  $-7\text{ kOe}$ , the shell vortex phase has a rather different profile. The shell vortex phase is seen in a larger fraction of the shell volume, covering a  $\pi$  wide belt centered at  $\theta = \pi/2$ . At the  $\theta \approx \pi/2$  belt the shell magnetization varies from near alignment with the core magnetization at the core-shell interface to the opposite direction at the shell surface.

The shell dipolar field in the core turns much stronger ( $\approx 4\text{ kOe}$  in most of the core), due to the larger shell volumes charges, associated with the variations in the magnetization within the shell. Notice that beyond the point of the shell vortex phase nucleation, the shell dipolar field enhances the stability of the uniform state of the core.

In Fig. 12 we compare the present results with the predictions of the average core-shell model, for  $\text{SmCo}_5(3.5\text{ nm})@Fe(\delta)$  and  $\text{SmCo}_5(21\text{ nm})@Fe(\delta)$  nanoparticles. The average core-shell model consists of assuming that the core-shell interface exchange energy suffices to keep core and shell magnetization parallel throughout the demagnetiza-

tion quadrant. Therefore, only coherent reversal is allowed. This theoretical strategy has been applied to investigate the main features of two-phase systems and multilayers composed of an aligned hard phase and a soft phase with high magnetization [24,25].

As we shall discuss, the simple average core-shell model has two major shortcomings. The relaxation of the shell magnetization, from the core-shell interface up to the shell surface is not allowed, and the core-shell dipolar interaction is not included. Therefore, we may anticipate that the validity of the simple average core-shell model is restricted to HSCS nanoparticles with small values of the core diameter and shell thickness.

In the average core-shell model the core-shell nanoparticle is represented in a macro-spin-like model, with the magnetization and the anisotropy energy density represented by the average values  $\langle M \rangle = f_c M_c + f_s M_s$ , and  $\langle K \rangle = f_c K_c + f_s K_s$ , where  $f_s$  and  $f_c$  are the shell and core volume fractions, and the coercive field is given by  $H_C = \frac{2\langle K \rangle}{\langle M \rangle}$ . Within this approximation, the reversal of magnetization occurs at the coercive field  $H_C$ , and the energy product is given by:

$$\langle BH \rangle_{\max} = \begin{cases} 4\pi^2 \langle M \rangle^2, & \text{if } H_C \geq 2\pi \langle M \rangle; \\ H_C(4\pi \langle M \rangle - H_C), & \text{if } H_C < 2\pi \langle M \rangle. \end{cases} \quad (2)$$

As seen in Figs. 12(a) and 12(b), the average core-shell model reproduces the present results for  $\delta < \delta^*$ . For this range of the Fe shell thicknesses, the magnitude of the external field for the nucleation of reversal  $H_N$  is larger than  $2\pi M$  and the critical field  $H^*$  reaches its optimum value  $H^* = 2\pi M$ . Thus, both models predict an energy product  $(BH)_{\max} = 4\pi^2 M^2$ . Notice that the average magnetization, used in the average core-shell model, is the saturation magnetization of the core shell, as used in the present model.

As shown in Figs. 4 and 8, for  $\delta > \delta^*$ ,  $H_N < 2\pi M$ . For this range of the Fe shell thicknesses, the average core-shell model fails in predicting the correct coercive field, since the dipolar interaction is not included. Furthermore, the average core-shell model does not allow for the large drop in the value of the magnetization, associated to noncoherent reversal.

As shown in Fig. 12(a) there are small differences between the predictions of the average core-shell model and the present theoretical model for the  $\text{SmCo}_5(3.5 \text{ nm})@Fe(\delta)$  nanoparticles. In this case, in both models, the magnetization reversal is coherent and the origin of the differences is the value of the coercivity. The average core-shell model does not account for the core-shell dipolar interaction, and, as a result, the values of the coercive field are larger than those found with the present theoretical model.

The differences between the predictions of the average core-shell model and the present theoretical model are much larger for the  $\text{SmCo}_5(21 \text{ nm})@Fe(\delta)$  nanoparticles. As seen in Fig. 12, the average core-shell model predicts an optimum Fe shell thickness value of  $\delta^* = 3 \text{ nm}$  for the  $\text{SmCo}_5(3.5 \text{ nm})@Fe(\delta)$  nanoparticles, in satisfactory agreement with the present theoretical model ( $\delta^* = 2.5 \text{ nm}$ ).

For the  $\text{SmCo}_5(21 \text{ nm})@Fe(\delta)$  nanoparticles the average core-shell model predicts an optimum Fe shell thickness of  $\delta^* = 19 \text{ nm}$ . This value is much larger than the value predicted by the present theoretical model ( $\delta^* = 4 \text{ nm}$ ).

In summary, we have discussed the magnetic phases, the reversal mechanisms, and the energy product of  $\text{SmCo}_5(D)@Fe(\delta)$  core-shell nanoparticles with  $\text{SmCo}_5$  core diameter ( $D$ ) ranging from 3.5 nm to 21 nm, and Fe shell thicknesses ( $\delta$ ) up to 8 nm. We have shown that the impact of the core-shell dipolar interaction on the magnetic phases in the demagnetization quadrant and the energy product is, to a large extent, controllable by the values of the core diameter and the shell thickness.

We have used the room temperature parameters [26] and reproduced satisfactorily the measured magnetization curve in the demagnetizing quadrant and the maximum energy product (28.6 MGOe) of  $\text{SmCo}_5$  magnets at room temperature [15], as seen in Figs. 2, 5, 7, and 12. We notice that high temperature effects might be an issue for future careful investigation. One might expect weak temperature effects for the  $\text{SmCo}_5$  core magnetic properties, with a critical blocking size of 2.24 nm, due to the large value of anisotropy, and a large Curie temperature of 1020 K [2]. However, regarding the iron shells the picture is not so clear. Although the Curie temperature of iron (1044 K) is also large [15] the iron anisotropy is not large. Therefore, the thermal stability of small volume iron shells is a point to be discussed. On one hand, one might envisage superparamagnetic behavior of thin iron shells on small diameter  $\text{SmCo}_5$  cores. On the other hand, thin iron shells may turn to be thermally stabilized via a strong interface coupling with the  $\text{SmCo}_5$  core [27]. This discussion is beyond the scope of the present paper.

Table II contains a summary of our results, focusing on the maximum energy product of  $\text{SmCo}_5(3.5 \text{ nm})@Fe(\delta \text{ nm})$  and  $\text{SmCo}_5(21 \text{ nm})@Fe(\delta \text{ nm})$  core-shell nanoparticles. As shown, the large core diameter nanoparticle exhibits the strongest dipolar effects, with larger differences between the theoretical maximum energy product and the value predicted by the present theoretical model.

We have found the optimum shell thickness which leads to the best core-shell composition for each of the chosen values of the  $\text{SmCo}_5$  core diameter. We have shown that the maximum energy product  $(BH)_{\text{max}}$  is a decreasing function of the core diameter value, dropping from 106.3 MGOe for the 3.5 nm

TABLE II. Nucleation field ( $H_N$ ), critical field ( $2\pi M$ ) and energy product maximum of  $\text{SmCo}_5(D)@Fe(\delta)$  core-shell nanoparticles.

$\text{SmCo}_5(3.5 \text{ nm})@Fe(\delta)$					
$\delta(\text{nm})$	$H_N$ (kOe)	$2\pi M$ (kG)	$(BH)_{\text{max}}$ (MGOe)	$4\pi^2 M^2$ (MGOe)	$\langle BH \rangle_{\text{max}}$ (MGOe)
0.0	400.0	5.4	28.6	28.6	28.6
0.5	143.0	8.4	69.5	69.5	66.8
1.0	66.0	9.49	88.2	88.2	86.6
1.5	35.3	9.9	97.6	97.6	97.0
2.0	21.0	10.1	103.0	103.0	102.8
2.5	12.7	10.3	106.3	106.3	106.3
3.0	9.0	10.4	105.6	108.7	108.5
3.5	6.7	10.5	92.7	110.0	104.2
4.0	5.0	10.5	76.5	110.9	92.8
4.5	3.8	10.6	66.3	111.6	80.6
5.0	3.1	10.6	51.3	112.1	69.7
$\text{SmCo}_5(21 \text{ nm})@Fe(\delta)$					
$\delta(\text{nm})$	$H_N$ (kOe)	$2\pi M$ (kG)	$(BH)_{\text{max}}$ (MGOe)	$4\pi^2 M^2$ (MGOe)	$\langle BH \rangle_{\text{max}}$ (MGOe)
0.0	400.0	5.3	28.6	28.6	28.6
1.0	126.0	6.6	43.1	43.9	43.9
2.0	52.0	7.5	55.8	56.6	56.6
3.0	22.5	8.2	66.2	66.8	66.8
4.0	10.8	8.6	74.1	74.9	75.0
5.0	5.5	9.0	66.2	81.4	81.4
6.0	2.5	9.3	39.6	86.6	86.6
7.0	1.0	9.5	24.3	90.8	90.8

core diameter  $\text{SmCo}_5(3.5 \text{ nm})@Fe(\delta)$  nanoparticles, for an optimum Fe shell thickness  $\delta = 2.5 \text{ nm}$ , to 74.1 MGOe for the 21 nm core diameter  $\text{SmCo}_5(21 \text{ nm})@Fe(\delta)$  nanoparticles, for an optimum Fe shell thickness  $\delta = 4.0 \text{ nm}$ .

Small core diameter  $\text{SmCo}_5@Fe$  nanoparticles are less vulnerable to the core-shell dipolar interaction effects and may be tailored to achieve a large enhancement of the energy product. The key point is that using thin Fe shells, one may reach large shell percentage volume fractions, and relevant enhancement of the energy product, as reported for small core diameters  $\text{FePt}@Fe_3O_4$  core-shell nanoparticles [8,17].

Large core diameter nanoparticles require thicker shells for energy product optimization. The large value of the core perimeter and the thicker shell thickness lead to noncoherent reversal, posing a limit on the value of the maximum energy product.

We have shown that the competition between the interface exchange and the dipolar energies, for large core diameter values, may lead to the formation of a new magnetic phase, the shell vortex phase. The shell vortex phase consists of a uniformly magnetized  $\text{SmCo}_5$  core with the Fe shell displaying a curling magnetization pattern that resembles the vortex phase of soft ferromagnetic materials. We have discussed the impact of the shell vortex phase in the magnetic phases in the demagnetization quadrant and in the energy product of  $\text{SmCo}_5(11 \text{ nm})@Fe(\delta)$  and  $\text{SmCo}_5(21 \text{ nm})@Fe(\delta)$  nanoparticles.

We have shown that a 3.5 nm core diameter  $\text{SmCo}_5(3.5 \text{ nm})@Fe(\delta)$  nanoparticle has an optimum shell thickness of  $\delta^* = 2.5 \text{ nm}$  and an energy product of 106.3 MGOe, which is 3.7 larger than that of the theoretical maximum value of the energy product ( $4\pi^2 M^2$ ) of the  $\text{SmCo}_5$  core (28.6 MGOe) and twice as large as that of NdFeB magnets [23]. The percentage shell volume fraction of the  $\text{SmCo}_5(3.5 \text{ nm})@Fe(2.5 \text{ nm})$  nanoparticle is 93% and the saturation magnetization is 1641 emu/cm<sup>3</sup>.

In order to reach a percentage shell volume fraction of 93%, a 21 nm core diameter  $\text{SmCo}_5(21 \text{ nm})@Fe(\delta \text{ nm})$  nanoparticle requires an Fe shell thickness of  $\delta = 15 \text{ nm}$ . This would lead to a rather small energy product value, due to the nucleation of the shell vortex phase in the demagnetization quadrant. The 21 nm core diameter  $\text{SmCo}_5(21 \text{ nm})@Fe(\delta)$  nanoparticle has an optimum shell thickness of  $\delta^* = 4.0 \text{ nm}$ , corresponding to

a percentage shell volume fraction of only 62% and an energy product of 74.1 MGOe.

We have discussed the average core-shell nanoparticle model, consisting of a macro-spin-like model, with the magnetization and the anisotropy energy density represented by the average values of the core and shell magnetic parameters, weighted by the corresponding volume fractions. We have shown that the validity of the average HSCS nanoparticle model is restricted to small values of the core diameter and shell thickness.

#### ACKNOWLEDGMENT

The authors acknowledge support from CNPq, CAPES, and FAPERJ. The work of A.S.C. and A.L.D. were supported by CNPq Grants No. 310785/2015-4 and No. 309929/2015-6.

- 
- [1] A. López-Ortega, M. Estarder, G. Salazar-Alvarez, A. G. Roca, and J. Nogués, *Phys. Rep.* **553**, 1 (2015).
  - [2] N. Poudyal and J. P. Liu, *J. Phys. D: Appl. Phys.* **46**, 043001 (2013).
  - [3] N. Poudyal, C. Rong, V. V. Nguyen, and J. P. Liu, *Mater. Res. Express* **1**, 016103 (2014).
  - [4] B. Balamurugan, D. J. Sellmyer, G. C. Hadjipanayis, and R. Skomski, *Scr. Mater.* **67**, 542 (2012).
  - [5] J. Sort, S. Surinach, J. S. Muñoz, M. D. Baro, J. Nogues, G. Chouteau, V. Skumryev, and G. C. Hadjipanayis, *Phys. Rev. B* **65**, 174420 (2002).
  - [6] V. Nandwana, G. S. Chaubey, K. Yano, C.-B. Rong, and J. P. Liu, *J. Appl. Phys.* **105**, 014303 (2009).
  - [7] Y. K. Hong and S. Bae, Magnetic exchange coupled core-shell nanomagnets, US20130342297 A1 (2013).
  - [8] F. Liu, J. Zhu, W. Yang, Y. Dong, Y. Hou, C. Zhang, H. Yin, and S. Sun, *Angew. Chem., Int. Ed.* **53**, 2176 (2014).
  - [9] H. Zeng, J. Li, J. P. Liu, Z. L. Wang, and S. Sun, *Nature (London)* **420**, 395 (2002).
  - [10] B. D. Cullity and C. D. Graham, *Introduction to Magnetic Materials* (Wiley, Piscataway, NJ, 2009), Chap. 13.
  - [11] F. F. Oliveira, T. R. S. Moura, A. S. Carriço, A. L. Dantas, and G. O. G. Rebouças, *J. Appl. Phys.* **111**, 07D102 (2012).
  - [12] C. M. Souza, A. L. Dantas, I. S. Queiroz, Jr., and A. S. Carriço, *J. Appl. Phys.* **115**, 17D110 (2014).
  - [13] L. L. Oliveira, M. S. Nunes, C. M. Souza, A. L. Dantas, I. Q. Souza, Jr., G. O. G. Rebouças, and A. S. Carriço, *IEEE Trans. Magn.* **51**, 1 (2015).
  - [14] F. C. M. Filho, L. L. Oliveira, S. S. Pedrosa, G. O. G. Rebouças, A. S. Carriço, and A. L. Dantas, *Phys. Rev. B* **92**, 064422 (2015).
  - [15] J. M. D. Coey, *Magnetism and Magnetic Materials* (Cambridge University Press, New York, 2009), Chaps. 7 and 11.
  - [16] P. O. Jubert, *IEEE Trans. Magn.* **50**, 3002004 (2014).
  - [17] H. Zeng, J. Li, Z. L. Wang, J. P. Liu, and S. Sun, *Nano Lett.* **4**, 187 (2004).
  - [18] Q. Song and Z. J. Zhang, *J. Am. Chem. Soc.* **134**, 10182 (2012).
  - [19] Y. Choi, J. S. Jiang, Y. Ding, R. A. Rosenberg, J. E. Pearson, S. D. Bader, A. Zambano, M. Murakami, I. Takeuchi, Z. L. Wang, and J. P. Liu, *Phys. Rev. B* **75**, 104432 (2007).
  - [20] Y. Zhang, M. J. Kramer, C. Rong, and J. P. Liu, *Appl. Phys. Lett.* **97**, 032506 (2010).
  - [21] X. B. Liu and Z. Altounian, *J. Appl. Phys.* **111**, 07B526 (2012).
  - [22] R. Lardé, J.-M. Le Breton, A. Maître, D. Ledue, O. Isnard, V. Pop, and I. Chicinaş, *J. Phys. Chem. C* **117**, 7801 (2013).
  - [23] S. Sugimoto, *J. Phys. D: Appl. Phys.* **44**, 064001 (2011).
  - [24] R. Skomski and J. M. D. Coey, *Phys. Rev. B* **48**, 15812 (1993).
  - [25] J. M. D. Coey, *Solid State Commun.* **102**, 101 (1997).
  - [26] E. Stilp, J. Freudenberger, M. Seifert, A. K. Patra, S. Menzel, I. Mönch, L. Schultz, and V. Neu, *J. Magn. Magn. Mater.* **324**, 1711 (2012).
  - [27] A. S. Carriço and R. E. Camley, *Phys. Rev. B* **45**, 13117 (1992).